PNAS
www.pnas.org

Supplementary Information for

Insight into microtubule nucleation from tubulin-capping proteins

Valérie Campanacci, Agathe Urvoas, Soraya Cantos-Fernandes, Magali Aumont-Nicaise, Ana-Andreea Arteni, Christophe Velours, Marie Valerio-Lepiniec, Birgit Dreier, Andreas Plückthun, Antoine Pilon, Christian Poüs, Philippe Minard, and Benoît Gigant

Email: christian.pous@u-psud.fr or benoit.gigant@i2bc.paris-saclay.fr

This PDF file includes:

Supplementary Methods
Figs. S1 to S15
Table S1
References for SI reference citation

www.pnas.org/cgi/doi/10.1073/pnas.1813559116

Supplementary Methods

Proteins. The iiiA5 αRep was selected in the same screen as iE5 and iiH5, and the same protocol was used to produce and purified all the αReps used in this study. The Δ92 and ΔCter CopN variants were obtained by standard molecular biology and were produced and purified similarly to full length CopN and Δ84. The F3II DARPin was identified in the same screen as D1 and the same protocol was used to purify all the DARPins used in this study. $(TM\text{-}3)_2$ was generated by inserting a GGGGSGGGGS linker between monomers, following the protocol described for $(D1)_2$ (1). To construct $(iiH5)_2$, the C-cap of the first αRep was removed and a $(GGGGS)_3$-GGS motif was introduced to link the last internal HEAT repeat of this first iiH5 to the N-terminal end of the N-cap of the second one. The tandem constructs were produced and purified following the protocol used for the parental monovalent proteins. Tubulin was purified from ovine brain by two cycles of assembly in a high-molarity buffer followed by disassembly (2). Before use, an additional cycle of assembly and disassembly was performed to remove inactive protein.

Isothermal titration calorimetry (ITC). Calorimetric experiments were conducted at 20°C with a MicroCal ITC200 instrument (Malvern). All proteins were buffer-exchanged to 20 mM Pipes-K pH 6.8, 1 mM $MgCl_2$, 0.01 mM EGTA, 0.01 mM GDP and 75 mM KCl. Aliquots (2 μl) of iiiA5 or CopN constructs (130 to 160 μM concentrations) were injected into a tubulin solution at 12 or 15 μM concentration (cell volume, 0.24 ml). Analysis of the data was performed using the MicroCal Origin software provided by the manufacturer according to the one-binding-site model.

Crystallization and structure determination.

CopN–tubulin–iiiA5. Crystals of this ternary complex were obtained by vapor diffusion at 293 K in polyethylene glycol 400, 0.1 M Mes pH 6.5, and using the Δ84 CopN construct. Datasets were collected at 100 K at the Proxima-2 beamline (SOLEIL Synchrotron, Saint-Aubin, France) and processed with XDS (3), as implemented in the XDSME package (4). The structure was solved by molecular replacement with Phaser (5) using tubulin (pdb id 5EYP), CopN (pdb id 4P40) and the αRep-n4-a αRep (pdb id 3LTM) as search models.

Tubulin–TM-3. Tubulin–TM-3 was crystallized in polyethylene glycol 5000 monomethyl ether, 0.1 M Mes-K pH 6.0 and 150 mM $(NH_4)_2SO_4$. A complete data set was collected at the MASSIF-1 automatic beamline of the European Synchrotron Radiation Facility (Grenoble, France) (6) and processed up to 2.7 Å. The structure was solved by molecular replacement using tubulin and the A-C2 DARPin (pdb id 5EYP) as search models.

Tubulin–F3II–R1. Tubulin–F3II was crystallized as a ternary complex with R1, a stathmin-like domain protein designed to bind one tubulin molecule, in polyethylene glycol 5000 monomethyl ether, 0.1 M Mes-K pH 6.0, 150 mM $(NH_4)_2SO_4$ and 50 mM KCl. Diffraction data were collected at 100 K at the Proxima-1 beam line (SOLEIL Synchrotron). The diffraction was anisotropic (about 3.2 Å in one direction, 3.8 Å in a second direction and 6.5 Å in a third direction). Data were processed up to 3.5 Å resolution with XDS then corrected for anisotropy using the Staraniso server (7). The structure was solved by molecular replacement using tubulin (pdb id 5EYP) and the D2 DARPin (pdb id 4F6R) as search models.
Structures were refined with BUSTER (8) with iterative model building in Coot (9). Data collection and refinement statistics are reported in SI Appendix, Table S1. Figures of structural models were generated with PyMOL (www.pymol.org). The electrostatic potential surface was calculated using APBS (10) and rendered in PyMOL.

Microtubule assembly monitored by turbidimetry. Microtubule assembly was performed in M2G1 buffer (50 mM Mes-K, pH 6.8, 6 mM $MgCl_2$, 0.5 mM EGTA, 30% (v/v) glycerol) supplemented with 0.5 mM GTP in the case of GTP-tubulin, or in PMg buffer (80 mM Pipes-K, pH 6.8, 4 mM $MgCl_2$, 1 mM EGTA, 0.2 mM GMPCPP) in the case of GMPCPP-tubulin. It was initiated by raising the temperature from 5°C to 37°C and monitored at 350 nm with a Cary 50 spectrophotometer (Agilent Technologies), using a 0.7-cm path length cuvette. In presence of the F3II DARPin, because of a likely slow association, the tubulin:F3II mixture was first incubated at 37°C in M2G1 buffer then assembly was initiated by adding GTP. For some experiments, to mitigate aggregation issues, the M2G1 buffer was supplemented with 75 mM KCl.

TIRFM experiments. Stabilized GMPCPP-microtubule seeds were prepared as described in ref. (11) using 10% HiLyte488-labeled tubulin (Cytoskeleton Inc) and phosphocellulose-purified porcine brain tubulin (12) in the presence of 1 mM GMPCPP (Jena Biosciences). Nucleation, elongation and dynamic assays were performed using recombinant kinesin-1 heavy chain (KHC, Cytoskeleton Inc)-coated coverslips (13) using GMPCPP seeds and a mixture of CopN and tubulin (as indicated) containing 5% of TAMRA-labeled tubulin (Cytoskeleton Inc.) and 1 mM GTP. For the determination of microtubule polarity, KHC was first loaded with 0.1 mM ATP to record microtubule seed gliding. Then, gliding was stopped by flushing 1 mM AMPPNP (Sigma) in the observation chamber prior to microtubule elongation. TIRF recordings were performed using a Zeiss AxioObserver Z1 microscope with a 100X / 1.46 Plan-Apochromat objective

equipped with a Peltier cooled CoolSnap HQ2 CCD camera (Photometrics) (MIPSIT platform of the "Institut Paris-Saclay d'Innovation Thérapeutique").

GTPase activity of tubulin. First, tubulin was loaded with GTP. To do so, tubulin (about 250 μM) was incubated with 3 mM GTP in 12.5 mM Mes-K pH6.8, 6 mM $MgCl_2$ for 30 min on ice. Excess nucleotide was removed by gel filtration on micro bio-spin P6 column (Bio-Rad). The percentage of GTP-loaded tubulin was estimated to be 91 ± 3% (n=3) (Fig. 6B, "starting material" curve). Then GTP hydrolysis was assessed both in microtubule assembly conditions (in M2G1 buffer and at 37°C) and in non-assembly conditions (incubation at room temperature in 60 mM Mes-K pH 6.8, 2 mM $MgCl_2$, 0.5 mM EGTA). At different time points, aliquots of tubulin and of CopN–tubulin were treated with trifluoroacetic acid and the denatured protein was removed by centrifugation. The pH of the supernatant containing released nucleotide was neutralized and the mixture was loaded on a mono Q anion exchange column (GE Healthcare) equilibrated with 20 mM Bis-Tris pH 6.0. Nucleotides were eluted using a 0 to 400 mM NaCl linear gradient, with GDP eluting at about 10.8 and GTP at about 12.3 ml. In the case of the CopN:tubulin sample, an additional chromatographic peak was observed at about 11.5 ml and corresponded to CopN that resisted denaturation by trifluoroacetic acid (Fig. 6B). The area of the chromatographic peaks recorded at 253 nm was calculated using the Unicorn software (GE Healthcare). The percentage of GDP- and GTP-tubulin was estimated assuming that half of the nucleotide signal comes from the non-hydrolysable GTP bound to α-tubulin.

Nucleation assays. During assembly of 4 μM GMPCPP-tubulin or of 12 μM GMPCPP-tubulin with 8 μM CopN, aliquots were withdrawn at different time points and immediately diluted (1:20 v/v) in PMg buffer supplemented with 1 μM Taxol at room temperature. The samples were infused in microchambers coated with constitutively active recombinant kinesin-1 heavy chain loaded with AMPPNP to prevent gliding (13). After fixation using ice-cold methanol, microtubules were processed for the indirect immunofluorescence labelling of tubulin using the mouse monoclonal DM1-A anti-alpha-tubulin antibody (Sigma).

Image analysis. The quantification of images from all the assays were performed using ImageJ software. Microtubule lengths were measured using the "AnalyzeSkeleton" plugin (14). The frequency distributions of the microtubule lengths at different times were compared within control or within CopN experiments using McNemar paired chi-square tests. Statistics for microtubule length distribution were from n=1722, n=2049 and n=2012 microtubules measured

on aliquots withdrawn at Abs_{350}=0.03 (one fourth of the plateau value), at Abs_{350}=0.06 (half of the plateau value) and at the turbidity plateau, respectively, in the case of the tubulin control (Fig. 1D). In the case of CopN:tubulin, the number of microtubules measured was n=989, n=1728 and n=1908, respectively (Fig. 1E). Dynamic instability parameters were measured from kymographs drawn in ImageJ.

Electron microscopy. Samples (3 μl) were deposited to a glow-discharged, carbon-coated copper grid and stained with 2% uranyl acetate. Data collection was performed using a Tecnai Spirit transmission electron microscope (FEI) equipped with a LaB6 filament, operating at 100 keV. Images were recorded using a K2 Base camera (Gatan, USA, 4k × 4k) at magnifications at the microscope from ×4400 to ×15000, which correspond to pixel size at specimen level from 0.83 to 0.25 nm, respectively.

Data availability. Coordinates and structure factors have been deposited in the Protein Data Bank under accession codes 6GX7 (CopN–tubulin–iiiA5), 6GVM (Tubulin–F3II–R1), and 6GVN (Tubulin–TM-3) (Table S1). Data supporting the findings of this study are available from the corresponding authors upon reasonable request.

Supplementary Figures

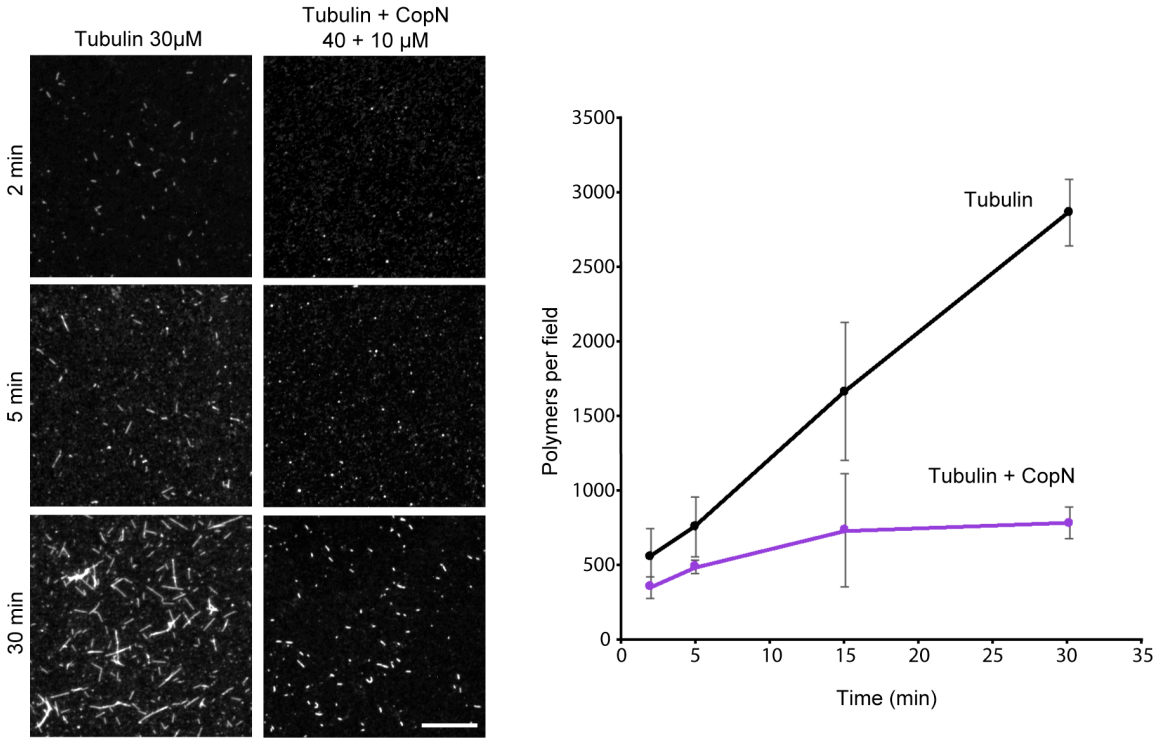

Figure S1. CopN inhibits microtubule nucleation. (Left) Fluorescence images of microtubules nucleated from GTP-tubulin or from GTP-tubulin:CopN solutions in M2G1 buffer and fixed at different time points, as indicated. (Right) Variation of the number of microtubules. Error bars, s.d.

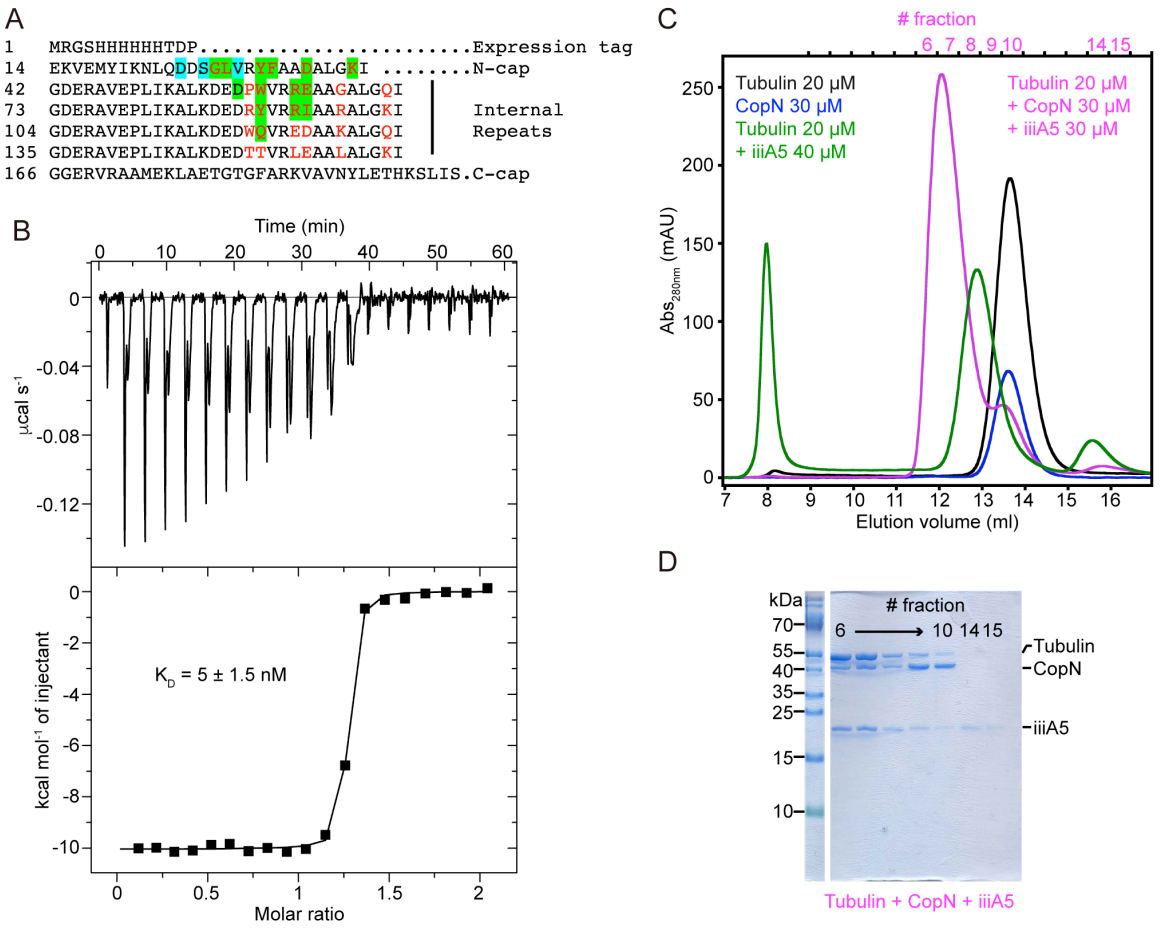

Figure S2. The iiiA5 αRep protein and its interaction with tubulin. (A) Sequence of iiiA5. The residues at randomized positions are in red. The iiiA5 residues that are less than 5 Å distant from tubulin residues in the CopN–tubulin–iiiA5 structure (Fig. 2D) are highlighted in cyan (invariant residues) or in green (randomized positions). (B) ITC titration (upper panel) and fitting curves (lower panel) of iiiA5 αRep with tubulin, from which a K_D of 5 ± 1.5 nM was extracted. (C) Gel filtration profile of tubulin, of CopN, of tubulin:iiiA5 and of CopN:tubulin:iiiA5 samples at the indicated concentrations. In the case of tubulin:iiiA5, aggregates eluting in the void volume of the column (at about 7.9 ml) are detected. (D) Fractions labelled at the top of panel C were submitted to SDS-PAGE, which indicates that iiiA5 makes a ternary complex with tubulin and CopN. Irrelevant lanes have been removed from the gel.

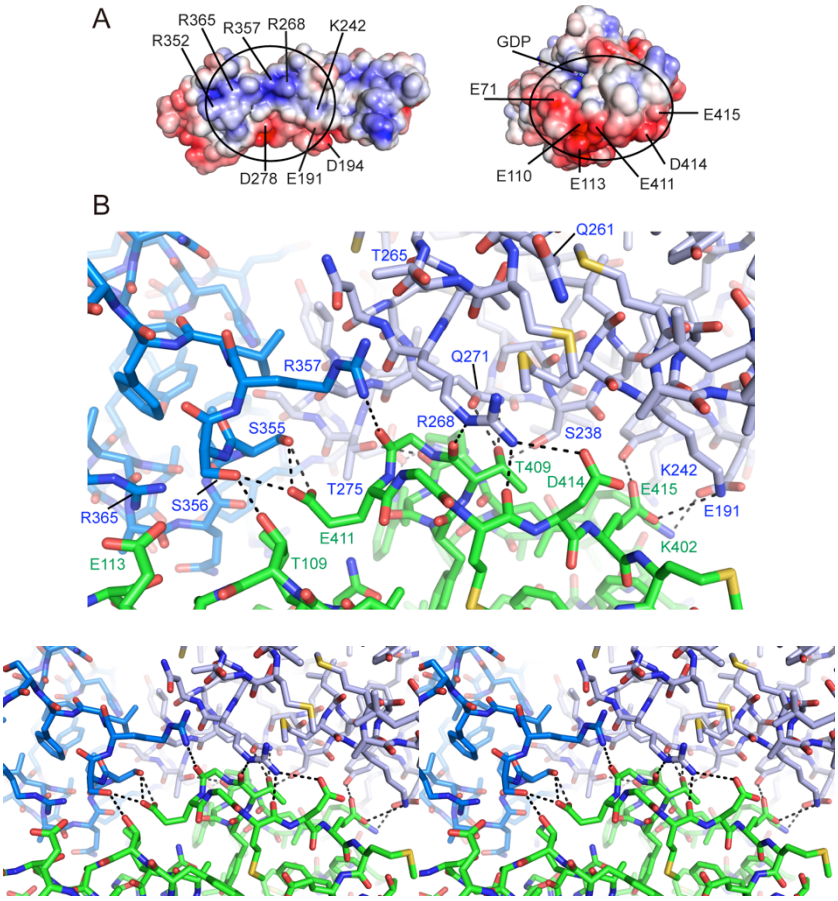

Figure S3. The CopN:tubulin interface. (A) Electrostatic potential surface of CopN (Left) and of tubulin (Right), with the interacting surfaces circled. Note that CopN and β-tubulin are both rotated by 90°, but in opposite directions, compared to Fig. 2D. (B) Close-up of the CopN:tubulin interface (Top, mono version; Bottom, stereo view). β-tubulin is in green and CopN is in different shades of blue as in Fig. 2D. The CopN–tubulin structure agrees with the effect of CopN mutations. For instance, R268, whose replacement by a His residue leads to an inactive CopN variant, interacts with the turn connecting the two C-terminal H11 and H12 helices of β-tubulin, and in particular with D414. Similarly, the S238E-K242E and Q271E-T275E double mutants, which are also inactive CopN variants, involve residues that are at the interface with tubulin. In particular, K242 together with the CopN residue E191, at one edge of the interacting surface, face residues E415 and K402 on the tubulin side. Finally, the CopN residues Q261 and T265, whose mutation to glutamate has a mild effect, are farther away from tubulin in the complex.

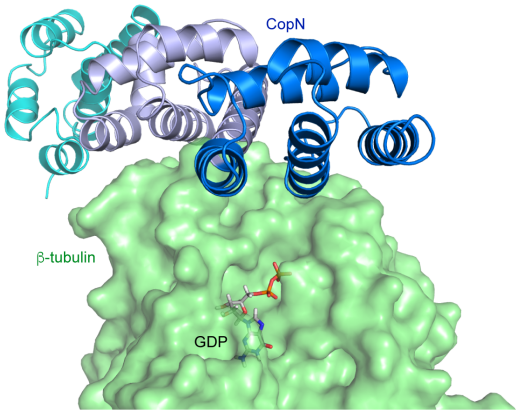

Figure S4. CopN binds at a distance from the β-tubulin nucleotide binding site.

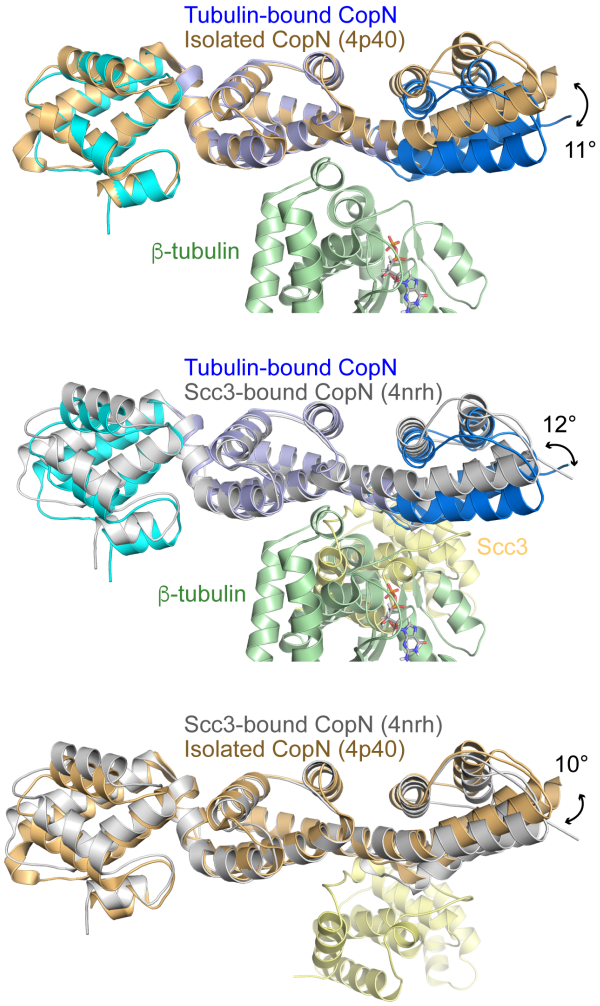

Figure S5. CopN structural changes upon tubulin binding. (Top) The second helical motif of isolated CopN (pdb id 4P40) has been superposed to that of CopN in complex with tubulin. To superimpose the third motifs, a rotation of about 11° of one motif with respect to the other one is needed. (Middle) Same as in the top panel but the comparison is with CopN bound to the Scc3 chaperone (pdb id 4NRH). After superposition of the second motifs, the third ones are misaligned by an angle value (12°) of similar amplitude to that in the top panel, but rotations are around different axes. This figure also indicates an overlap of the CopN binding sites for Scc3 and for tubulin. (Bottom) The mobility of the domains was already apparent from structures of CopN in the absence of tubulin, as shown with the superposition of isolated CopN and Scc3-bound CopN on their second helical motif.

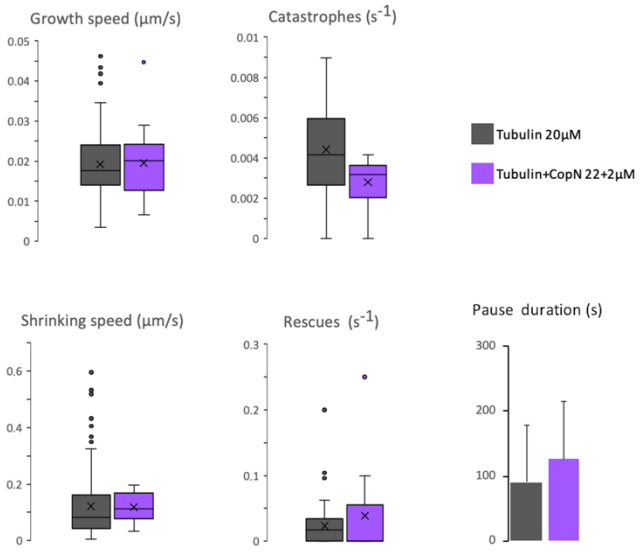

Figure S6. A low concentration of CopN does not alter dynamic instability parameters upon addition to dynamic microtubules. The parameters shown were quantified from TIRF microscopy experiments. The values plotted as box and whisker graphs (10, 25, 50, 75 and 90 percentiles plus outlier values, n comprised between 13 and >180 values) were derived from kymographs that were drawn from time-lapse sequences taken during the first 15 min that followed the addition of CopN, as reported in Figure 3C. The measurements correspond to the behavior of microtubule (+) ends, which were distinguished from (-) ends, based on their higher elongation speed.

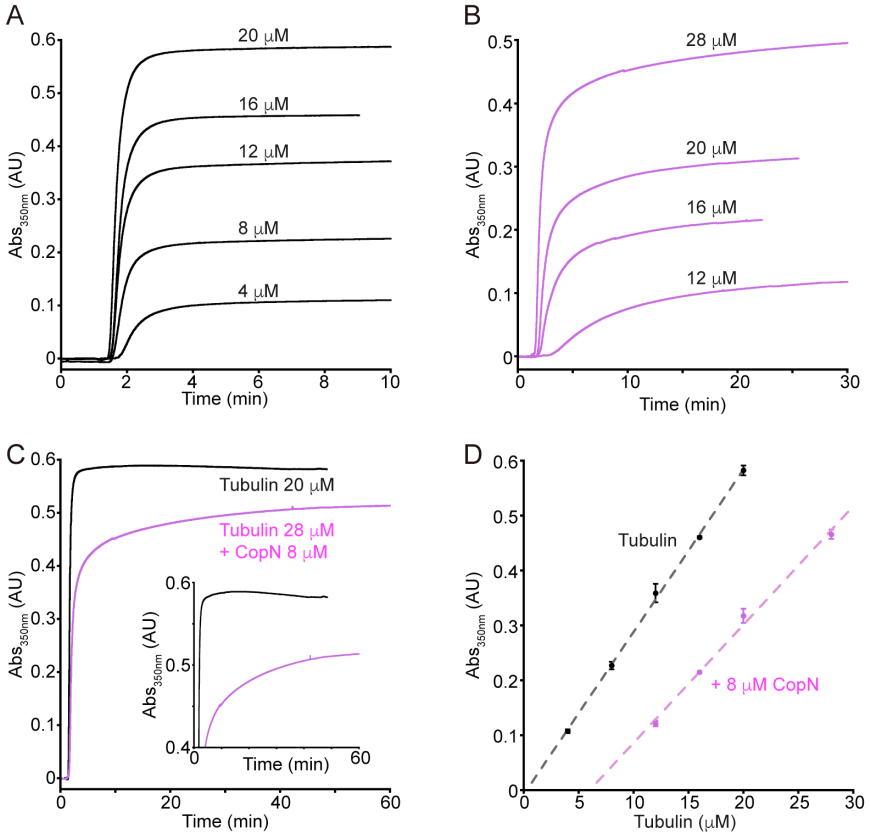

Figure S7. Effect of CopN on the assembly of GMPCPP-tubulin monitored by turbidity. (A) Assembly in PMg buffer of GMPCPP-tubulin at the indicated concentrations. The temperature was switched from 5°C to 37°C after one minute of recording time. (B) Same experiments as in panel A, but in the presence of 8 μM CopN. (C) Assembly curve of a 8:28 μM CopN:tubulin sample recorded during one hour and comparison with a 20 μM tubulin control. Inset, zoom on the plateau. (D) Critical concentration plots for microtubule assembly of GMPCPP-tubulin and of GMPCPP-tubulin in presence of 8 μM CopN. The absorbance signal reported in the case of the tubulin:CopN samples was taken 10 minutes after the start of the "drifting" phase of the turbidity curves in panel B. The derived critical concentration of GMPCPP-tubulin (abscissa intercept) is about 0.25 μM. Error bars are s.d. from two experiments.

It was previously proposed that CopN inhibits microtubule elongation mainly through tubulin sequestration. Indeed, we found that critical concentration plots for microtubule assembly of GTP-tubulin in presence of CopN remained parallel to that of the GTP-tubulin control, pointing to a sequestration mechanism (15). However, a more complex mechanism is inferred from the TIRFM experiments (Fig. 3). To investigate this point further, we determined additional critical concentration plots but with GMPCPP-tubulin. In these conditions, the slope of the critical concentration curve in presence of 8 μM CopN is lower than that of tubulin (panel D). In addition, the turbidity of tubulin:CopN samples did not reach a stable plateau, different to the tubulin control case (panel C). Both indicate a CopN mechanism that is more complex than a tubulin sequestration one, in agreement with the TIRFM experiments. It is possible that the effect on the critical concentration plots is exacerbated with GMPCPP-tubulin compared to GTP-tubulin, which might explain why the conclusions reached here are different from previous ones.

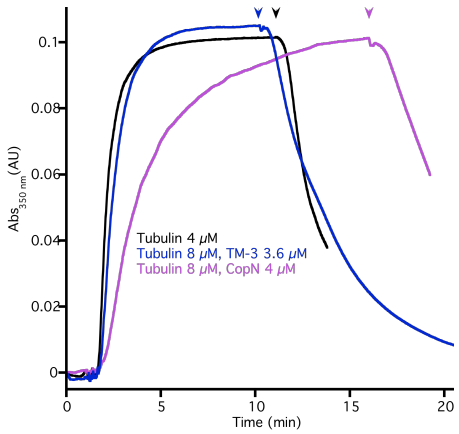

Figure S8. The TM-3 DARPin does not delay microtubule assembly of GMPCPP-tubulin. The turbidity trace in PMg buffer of GMPCPP-tubulin:TM-3 (blue curve) is shown together with those of tubulin and tubulin:CopN taken from Fig. 1A.

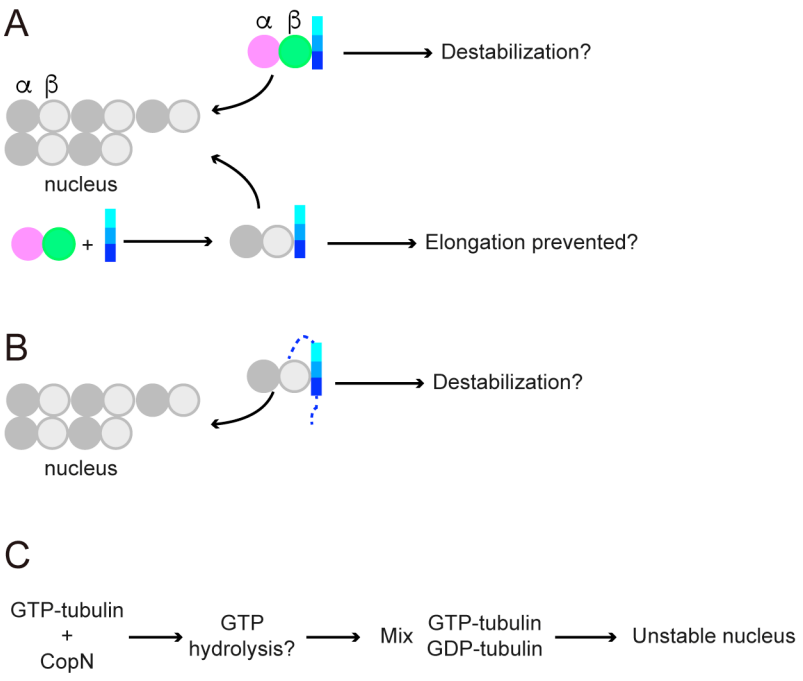

Figure S9. Hypotheses for the mechanism of microtubule nucleation inhibition by CopN. (A) Upper pathway: CopN might stabilize tubulin in a conformation (colored) not compatible with the one(s) in the nucleus (grey). In this case, the binding of such a tubulin (or a CopN molecule) to the nucleus might destabilize it. Lower pathway: alternatively, CopN might have a higher affinity for tubulin within the nucleus, hence preventing nucleus elongation. (B) The mobile regions of CopN (dashed extensions) might prevent the establishment of tubulin contacts within the nucleus. In panels A and B, the nucleus is represented in an arbitrary form. (C) CopN might trigger the hydrolysis of GTP, which has been shown to destabilize nucleation intermediates.

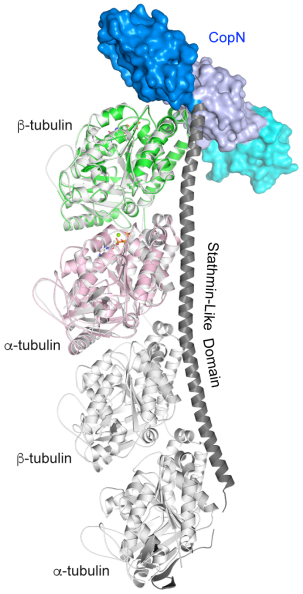

Figure S10. The structures of tubulin bound to CopN or to stathmin-like domain (SLD) proteins are similar. The structure of one tubulin of a T_2SLD complex (pdb id 3RYC (16)) has been superimposed to that of CopN–tubulin–iiiA5. The conformations of tubulin are very close in both complexes, with a r.m.s.d. of 0.778 Å (862 tubulin Cαs aligned), whereas SLDs act as pure tubulin-sequestering proteins (15). CopN–tubulin is colored as in Fig. 2D; iiiA5 is not shown. Tubulin from T_2SLD is in light grey; the SLD is in darker grey. This superposition also indicates that the C-terminal part of the SLD helix is in steric conflict with CopN, providing a rationale for the competition between SLDs and CopN for tubulin binding.

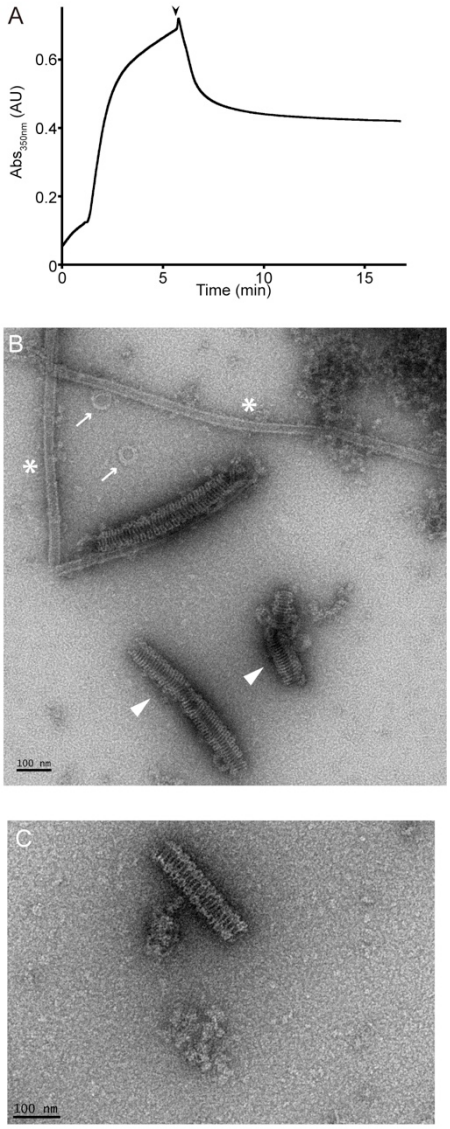

Figure S11. The iiiA5 αRep induces ring-like aggregates of tubulin. (A) Turbidity traces of tubulin:iiiA5 in M2G1 buffer supplemented with 0.5 mM GTP. (B,C) Electron micrographs of negatively-stained tubulin:iiiA5 incubated at 37 °C (B) and after cooling on ice (C). At 37 °C, microtubules (asterisks) coexist with isolated rings (arrows), stacked rings (arrow heads), and less-ordered ring-like aggregates (top right). After cooling, microtubules have disassembled, but the ring-like structures are still present, in agreement with the persistence of the turbidity signal in panel A after cooling to 5 °C. For both experiments, the tubulin concentration was 20 μM and that of iiiA5 was 12 μM. The samples were diluted 2-fold for grid preparation. Scale bar, 100 nm.

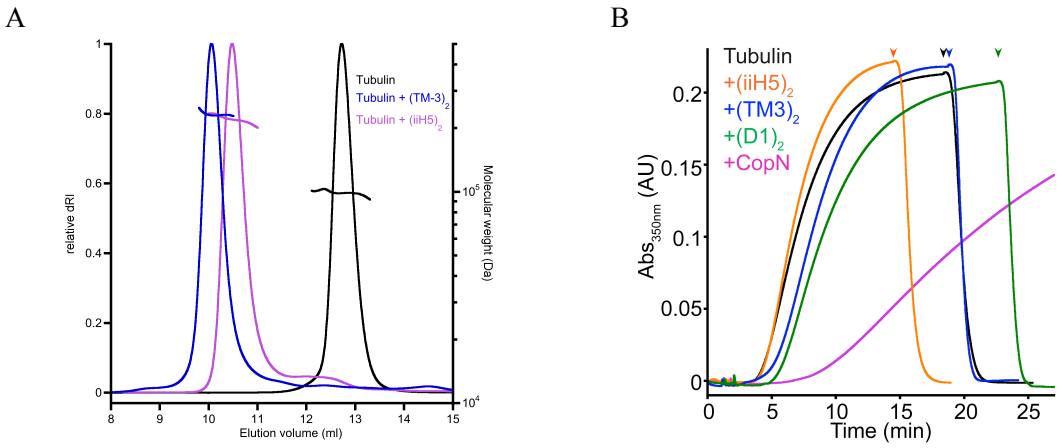

Figure S12. The $(D1)_2$, $(TM\text{-}3)_2$ and $(iiH5)_2$ tandem repeat proteins do not delay microtubule assembly. (A) $(TM\text{-}3)_2$ and $(iiH5)_2$ form with tubulin complexes having a 2:1 tubulin:divalent protein stoichiometry. Samples of 20 µM tubulin alone or with 20 µM $(TM\text{-}3)_2$ or $(iiH5)_2$ were analyzed by size exclusion chromatography on a Superdex 200 10/300 increase column (GE Healthcare) coupled to multi-angle laser light scattering in a buffer consisting of 20 mM Pipes-K, pH 6.8, 50 mM KCl, 1 mM $MgCl_2$, 0.5 mM EGTA. The differential refractive index (normalized dRI, left axis) and molecular mass (right axis) are plotted as a function of the column elution volume. Detection was performed using a three-detector static light-scattering apparatus (MiniDAWN TREOS, Wyatt Technology, equipped with a quasi-elastic light-scattering module) and a refractometer (Optilab T-rEX, Wyatt Technology). Calculations of the molecular weight were performed with the ASTRA 6 software (Wyatt Technology) using a dn/dc value of 0.183 ml/g. The derived masses are 98.6 ± 0.4 kDa for tubulin, 230.0 ± 0.4 kDa for tubulin:$(TM\text{-}3)_2$ and 220 ± 0.4 kDa for tubulin:$(iiH5)_2$. The mass of the complexes reasonably matches the one calculated from tubulin:construct complexes of stoichiometry 2:1, the theoretical molecular weight of $(TM\text{-}3)_2$ and of $(iiH5)_2$ being 35.4 kDa and 33.4 kDa, respectively. (B) The $(TM\text{-}3)_2$, $(D1)_2$, and $(iiH5)_2$ tandem repeat proteins do not delay nucleation. Tubulin (30 µM) was mixed with about 7.5 µM of the indicated tandem repeat protein in M2G1 buffer supplemented with 0.5 mM GTP and 75 mM KCl. Tubulin (15 µM) and tubulin:CopN (30:15 µM) curves are from Fig. 5B.

The experiments performed with CopN and DARPins suggest that proteins that may interfere with two protofilaments at the (+) end (e.g. CopN and D2) delay nucleation whereas those that target one protofilament (e.g. TM-3 and F3II) do not. In this experiment, we questioned whether a tandem repeat of TM-3, that may cap two protofilaments, impacts microtubule nucleation. For this purpose, we designed $(TM\text{-}3)_2$, a construct comprising two TM-3 moieties separated by a (GGGGS)2 linker. A similar construct in the case of D1 DARPin led to a $(D1)_2$ protein that inhibits microtubule (+) end elongation more efficiently than monovalent D1. We also studied a tandem $(iiH5)_2$ αRep, designed to cap two protofilaments at the (-) end. Whereas both $(TM\text{-}3)_2$ and $(iiH5)_2$ formed in solution complexes with tubulin having a 2:1 tubulin:divalent protein stoichiometry (panel A), they did not delay microtubule assembly in the turbidity assay (panel B). We also recorded the effect of $(D1)_2$ and found that it also has no appreciable effect either (panel B). These experiments suggest that either these divalent proteins are unable to cap two protofilaments in the context of the nucleus, or the capping of two protofilaments achieved by proteins consisting of two such flexibly linked partners does not impact nucleation.

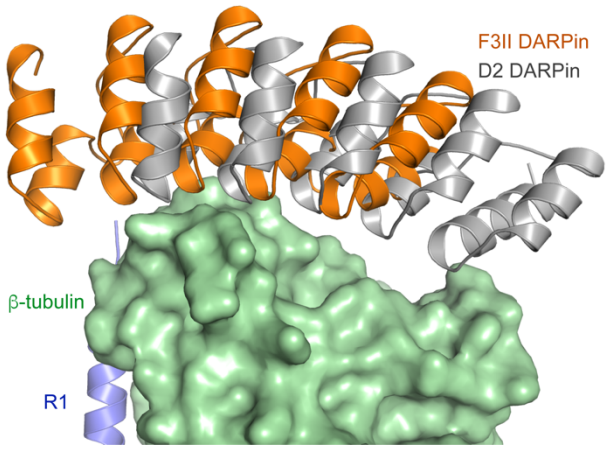

Figure S13. Comparison of the binding site of D2 and F3II DARPins on tubulin. The β subunit from tubulin–D2–R1 (pdb id 4F6R; only D2 is shown) has been superimposed to that of tubulin–F3II–R1. The two DARPins are similarly oriented on tubulin but are translated by about one ankyrin motif and a half.

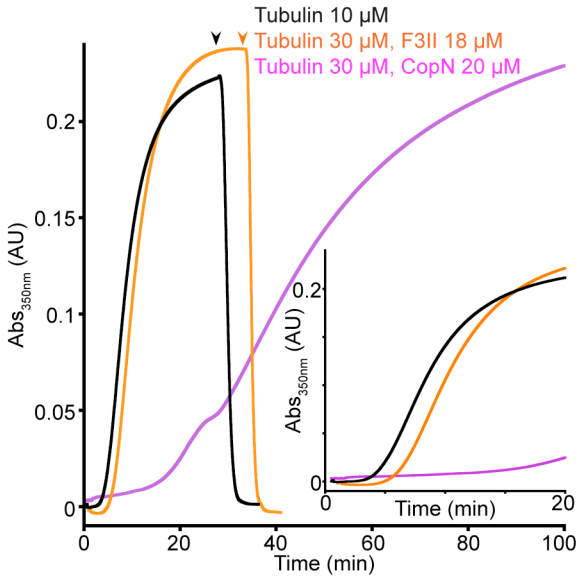

Figure S14. Pre-incubating tubulin and tubulin:CopN in M2G1 buffer does not change the microtubule assembly properties. This experiment is a control experiment related to the study of the F3II DARPin. This DARPin formed oligomers, eluting in an enlarged peak in the gel filtration step during purification. In addition, preliminary microtubule assembly experiments suggested a slow tubulin:F3II association, one explanation being that the rate of complex formation was limited by the dissociation of the oligomers. Therefore, to avoid this complication, we adapted the turbidity assay. We incubated beforehand the tubulin:F3II mixture for at least 10 minutes, then GTP was added to initiate the assembly kinetics. This figure shows that applying this procedure to tubulin or tubulin:CopN samples does not impact microtubule assembly. Tubulin and tubulin:CopN at the indicated concentrations were incubated 10 minutes in M2G1 buffer at 37 °C then GTP (0.5 mM) was added. The addition of GTP corresponds to the time origin. Tubulin:F3II from Fig. 7F is shown for comparison. Inset, zoom on the first 20 minutes of the experiment.

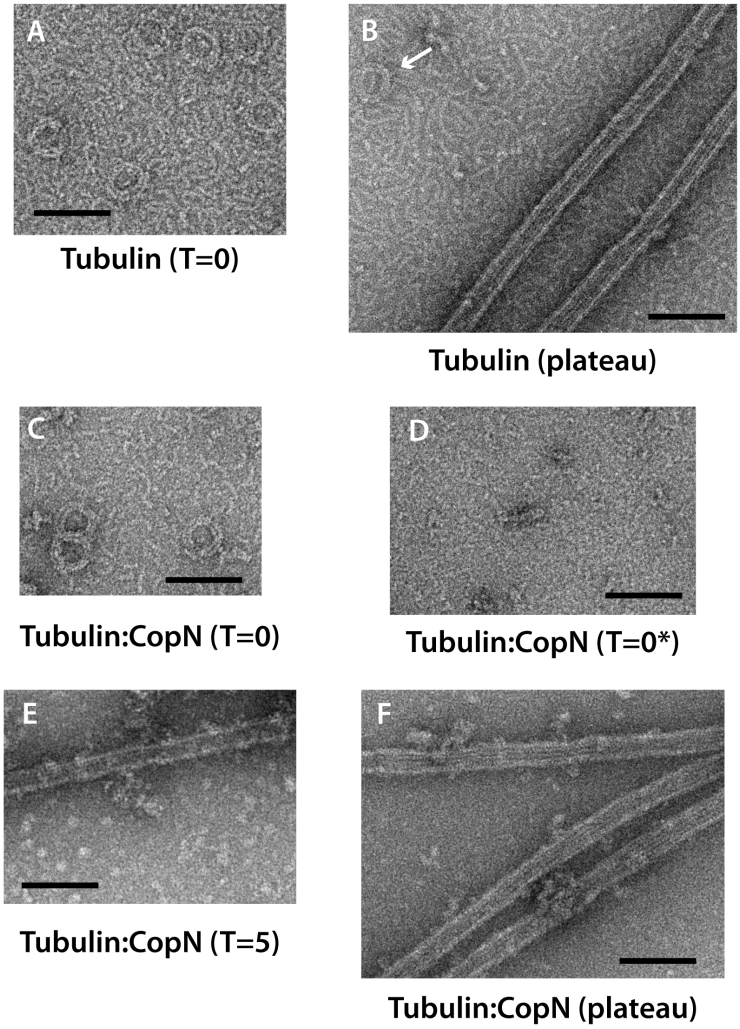

Figure S15. Electron micrographs of negatively-stained tubulin and tubulin:CopN samples. (A) Tubulin control, diluted to 30 μM from a 430 μM stock solution, and then further diluted 5-fold for grid preparation. (B) Tubulin (10 μM) incubated at 37 °C. (C-F) Samples of 30 μM tubulin and 20 μM CopN, diluted 5-fold for grid preparation. Tubulin rings are seen just after dilution from stock solutions in GTP-containing M2G1 assembly buffer, both in the tubulin control (A) and in the tubulin:CopN sample (C), in agreement with other studies (Ref 17 and ref therein) . Most of these rings disappear after incubation (e.g., panel D, incubation 15 min on ice), while some remain visible (B, arrow). In the tubulin:CopN sample, few microtubules are seen after 5 min incubation at 37 °C (E). More microtubules are seen after 25 min (Fig. 2C, inset) and at the turbidity plateau (F). These microtubules are indistinguishable from those obtained with tubulin alone (panel B). Scale bar, 100 nm throughout.

Supplementary Table

Table S1. Data collection and refinement statistics.

	CopN–tubulin–iiiA5	Tubulin–F3II–R1	Tubulin–TM-3
Data collection[(a)]			
Space group	$P2_1$	C2	$P2_1$
Cell dimensions			
a, b, c (Å)	148.1, 95.8, 158.1	189.3, 51.7, 144.1	73.1, 84.3, 82.0
α, β, γ (°)	90.0, 101.5, 90.0	90.0, 121.0, 90.0	90.0, 99.0, 90.0
Resolution (Å)	49.03-3.19 (3.30-3.19)	49.3-3.50 (3.73-3.50)	43.08-2.69 (2.79-2.69)
R_{meas}	0.2023 (1.545)	0.283 (1.89)	0.249 (1.167)
I / σI	7.37 (1.07)	5.8 (1.3)	6.2 (1.19)
$CC_{1/2}$	0.998 (0.404)	0.988 (0.258)	0.977 (0.668)
Completeness	0.99 (0.93)	0.501 (0.147)[(b)] 0.903 (0.77)[(c)]	0.983 (0.916)
Multiplicity	3.9 (3.8)	3.4 (3.4)	3.4 (3.4)
Refinement			
Resolution (Å)	49.03-3.19	49.3-3.50	43.08-2.69
No. reflections	72103	7763	26956
Rwork / Rfree	0.173 / 0.210	0.245 / 0.270	0.193 /0.216
No. atoms			
Protein	20123	8335	7680
Ligands	218	61	95
Solvent	0	0	115
B factors			
Protein	115.4	57.7	52.0
Ligands	96.7	28.0	45.1
Solvent			33.7
Coordinate error (Å)	0.38	0.65	0.39
R.m.s.d.			
Bond lengths (Å)	0.010	0.009	0.010
Bond angles (°)	1.16	1.07	1.15
Ramachandran (%)			
Favored region	96.64	97.27	96.14
Allowed region	2.94	2.73	3.25
Outliers	0.42	0	0.61

[(a)]Data were collected on a single crystal. Values in parentheses are for the highest-resolution shell.
[(b)]Spherical processing. [(c)]Ellipsoidal processing.

References for SI reference citation

1. Dreier B*, et al.* (2011) Her2-specific multivalent adapters confer designed tropism to adenovirus for gene targeting. *J Mol Biol* 405:410-426.
2. Castoldi M, Popov AV (2003) Purification of brain tubulin through two cycles of polymerization-depolymerization in a high-molarity buffer. *Protein Expr Purif* 32:83-88.
3. Kabsch W (2010) XDS. *Acta Crystallogr D Biol Crystallogr* 66:125-132.
4. Legrand P (2017) XDSME: XDS Made Easier. *GitHub repository* DOI 10.5281/zenodo.837885.
5. McCoy AJ*, et al.* (2007) Phaser crystallographic software. *J Appl Crystallogr* 40:658-674.
6. Bowler MW*, et al.* (2015) MASSIF-1: a beamline dedicated to the fully automatic characterization and data collection from crystals of biological macromolecules. *J Synchrotron Radiat* 22:1540-1547.
7. Tickle IJ*, et al.* (2018) STARANISO. Cambridge, United Kingdom: Global Phasing Ltd.
8. Bricogne G*, et al.* (2017) BUSTER version 2.10.3 Cambridge, United Kingdom: Global Phasing Ltd.
9. Emsley P, Lohkamp B, Scott WG, Cowtan K (2010) Features and development of Coot. *Acta Crystallogr D Biol Crystallogr* 66:486-501.
10. Baker NA, Sept D, Joseph S, Holst MJ, McCammon JA (2001) Electrostatics of nanosystems: application to microtubules and the ribosome. *Proc Natl Acad Sci U S A* 98:10037-10041.
11. Aher A*, et al.* (2018) CLASP suppresses microtubule catastrophes through a single TOG domain. *Dev Cell* 46:40-58 e48.
12. Walker RA*, et al.* (1988) Dynamic instability of individual microtubules analyzed by video light microscopy: rate constants and transition frequencies. *J Cell Biol* 107:1437-1448.
13. de Forges H*, et al.* (2016) Localized mechanical stress promotes microtubule rescue. *Curr Biol* 26:3399-3406.
14. Arganda-Carreras I, Fernandez-Gonzalez R, Munoz-Barrutia A, Ortiz-De-Solorzano C (2010) 3D reconstruction of histological sections: Application to mammary gland tissue. *Microsc Res Tech* 73:1019-1029.
15. Jourdain L, Curmi P, Sobel A, Pantaloni D, Carlier MF (1997) Stathmin: a tubulin-sequestering protein which forms a ternary T2S complex with two tubulin molecules. *Biochemistry* 36:10817-10821.
16. Nawrotek A, Knossow M, Gigant B (2011) The determinants that govern microtubule assembly from the atomic structure of GTP-tubulin. *J Mol Biol* 412:35-42.
17. Shemesh A, Ginsburg A, Levi-Kalisman Y, Ringel I, Raviv U (2018) Structure, assembly, and disassembly of tubulin single rings. *Biochemistry* 57:6153-6165.